# Constant Pressure Panel Method for Supersonic Unsteady Airload Analysis

K. Appa*
*Northrop Corporation, Hawthorne, California*

**A constant pressure panel method for computing the generalized aerodynamic forces on lifting surfaces in inviscid isentropic flow is discussed. An aerodynamic influence coefficient formulation relating the normal wash and the panel pressure distributions has been derived. The formulation is such that there is no need to consider the wake or the diaphragm elements in the analysis. Since there is no series expansion of the frequency term in this method, computations at low supersonic Mach numbers and high reduced frequencies can be performed with no convergence difficulties. In terms of the basic data and panel organization, the pressure panel method presented in this paper is similar to the doublet-lattice method used in the subsonic flow. Hence, it is possible to develop a unified computer code for analysis in subsonic and supersonic flow.**

## Introduction

MODERN fighters are being designed for high maneuverability and increased fatigue life. These design considerations are influenced by the aeroelastic stability of the aircraft. Accurate stability analyses can be performed, provided reliable means are available to compute unsteady aerodynamic forces in subsonic and supersonic flow regimes. For wing-like components, in subsonic flow, the doublet-lattice method (DLM) developed in Ref. 1 has been proven to predict the unsteady forces with a high degree of accuracy. However, its counterpart in supersonic flow does not exist. In the past, several numerical methods have been proposed. These are generally classified as source, velocity potential, velocity potential gradient, and acceleration potential methods.

The source superposition method gives a very simple integral relationship between the potential and the normal wash field (which is determined by the mode shapes) in the noninteracting case. However, in the interacting case, the potential is first related to the source strength, and this, in turn, is related to the downwash distribution. Thus, by this method, two sets of equations are involved in solving the problem. In addition, integration over wake regions and nonunique "diaphragms" are necessary as a part of the solution. Using this approach, Refs. 2 and 3 employed Mach box-type elements with their diagonals parallel to the Mach lines. This type of modeling results in discontinuous leading and trailing edges that emit artificial Mach waves. Across these Mach lines, spurious pressure jump will be generated. To eliminate such problems, Ref. 4 introduced a triangular element scheme to represent a true planform of a lifting surface.

In the velocity potential method, there is a direct relationship between the normal wash and the velocity potential. Diaphragm regions are no longer necessary but the wake regions still need to be modeled since their behavior is determined by the trailing-edge potentials of the wake-producing surface. The integral relations are more complicated than those in the source superposition method. Reference 5 employed a characteristic grid arrangement with quadratic expressions for the unknown potentials within each element, whereas Ref. 6 employed a general quadrilateral element scheme with linear variation of the potentials within each element. Both of these schemes have reported good prediction of the pressure distributions on general planforms. However, Ref. 6 seems to have recognized some sensitivity with respect to the panel arrangements.

To improve the computational stability and accuracy of the results, a higher-order potential scheme known as the potential gradient method (PGM) was introduced in Ref. 7. This scheme was further extended to cascade blades of compressors and turbines.[8] In this method, the kernel was expressed by a power series of the reduced frequencies. At high reduced frequencies, this method experienced convergence problems. Reference 9 employed a numerical integration scheme for the far-field elements, without expanding the kernel in a series form. As an alternative, Ref. 10 implemented a numerical integration scheme in which the exponential term was treated as a variable within the element. However, the potential gradient method required the modeling of the wake field extending from the trailing edge of the wing to the leading edge of the tail. Depending on the configuration, this region may be larger than the lifting surfaces.

A supersonic kernel function relating the pressure differential across a panel and the normal wash was derived by Harder and Rodden.[11] Several numerical schemes employing some variation of the kernel of Ref. 11 have been developed. For example, Ref. 12 employed a collocation scheme to determine the normal wash due to a known pressure mode. Several intriguing discussions on the handling of the singular kernel along the Mach boundary are presented in this reference. Although very good results are obtained by using this method, it requires the knowledge of the pressure mode resulting from steady flow analysis, which may be difficult to predict in complex configurations. Thus this computational scheme lacks generality.

Reference 13 applied the doublet-lattice-type scheme employed in the subsonic case, but using a slightly modified form of the kernel of Ref. 11. This approach encountered the problem of singularities along the Mach boundaries. An alternative approach uses a doublet-point method using the supersonic kernel function, a slightly modified form of Ref. 11, for planar configurations. The authors expressed the supersonic kernel as steady and unsteady parts. The steady part was integrated over an equivalent rectangular box, while the unsteady part was evaluated at a single point. Since the equivalent rectangular elements are used, the leading and trailing edges of a tapered wing will be approximated by sharp edges, which, in turn, will

Presented as Paper 85-0596 at the AIAA/ASME/ASCE/AHS 26th Structures, Structural Dynamics and Materials Conference, Orlando, FL, April 15-17, 1985; received June 22, 1986; revision received Jan. 29, 1987. 

*Senior Technical Specialist. Aircraft Division.

result in similar chordwise pressure oscillations, as obtained by the Mach box method and exhibited in Fig. 12 of Ref. 14. At high reduced frequencies, the supersonic kernel varies significantly in the chord direction of an element. Hence, evaluation of this function at a single point either produces error in the computed pressures if a small number of chordwise elements are used or requires a substantial number of chordwise elements for reasonable accuracy.

Another collocation method similar to that described in Ref. 12 has been investigated in Ref. 15. This approach assumes a polynomial distribution of the pressure within a region bounded by Mach lines. The coefficients of the polynomial are determined by satisfying the normal wash at the central points. The normal wash was determined by means of finite differentiation with excellent agreement with other methods of computing the normal velocity. Since this method also requires the knowledge of a region bounded by Mach lines, its application to general planforms is limited.

The present method describes a simple approach to derive an integral relation between the pressure and the normal velocity, based on the potential gradient method discussed in Ref. 7. A rearrangement of the exponential term associated with the kernel of the potential gradient resulted in the pressure differential as a new variable. The new kernel associated with the pressure also contains the hyperbolic singularity along the Mach boundary. In the present approach, this singularity is avoided by first integrating the kernel in the streamwise direction. The resulting function then takes a finite value on the Mach boundary. Hence, the computed normal velocity is finite and continuous at any control point. A similar treatment of the kernel has been employed in Ref. 7 to obtain the closed-form expressions for the velocity components. For the nonplanar case, the second part of the integral has been obtained by using the numerical differentiation of the first term. This eliminates the laborious computation of the kernel. Since there exists a direct relation to the pressure and the displacements, similar to that observed in the doublet-lattice method widely used in the subsonic flow, the present algorithm can be implemented within the doublet-lattice code, so that a unified code would then be available for subsonic and supersonic flow analyses.

To verify the accuracy and applicability of the method for general planforms and interfering cases, a few examples have been computed using AGARD planforms, for which results are available from other sources. The correlations are very encouraging. The subsequent sections describe the analytical formulation and the discussion of the computed results.

## Formulation of the Integral Equations

The linearized equation of motion of a fluid medium is given by

$$\nabla^2\phi' = \frac{1}{a^2}\frac{\mathrm{D}^2\phi'}{\mathrm{D}t^2} \tag{1}$$

where $\phi'$ is the velocity potential, $a$ the speed of sound, and

$$\frac{\mathrm{D}}{\mathrm{D}t}(\ ) = \frac{\partial}{\partial t} + V\frac{\partial}{\partial x} \tag{2}$$

is a substantial derivative. Let

$$\Phi = \phi \exp\left(i\frac{kM^2X}{\beta^2}\right) \tag{3}$$

be a modified velocity potential, $\phi = \phi'/V\ell$ a nondimensional velocity potential, and

$$X = x/\ell, \quad Y = y/\ell, \quad Z = z/\ell, \quad T = Vt/\ell \tag{4}$$

the nondimensional space coordinates and time in which $\ell$ is a reference length.

Then the solution to Eq. (1), according to Jones,[16] is given by

$$\Phi(\chi_0) = E\iint K'(\chi)\frac{\partial}{\partial n}\frac{\cos k'R}{R}\,\mathrm{d}A \tag{5}$$

where

$\chi_0$ = control point, $= (X_0, Y_0, Z_0)$

$\chi$ = domain of dependence, $= (X, Y, Z)$

$R^2 = \xi^2 - \beta^2 r^2$

$r^2 = \eta^2 + \zeta^2$

$k$ = reduced frequency, $= \omega\ell/V$

$k' = kM/\beta^2$

$K'$ = modified potential doublet, $= \phi_U - \phi_L$

$E = 1/(2\pi)$

$$\frac{\partial}{\partial n} = -\ell_x\frac{\partial}{\partial x} + \ell_y\frac{\partial}{\partial y} + \ell_z\frac{\partial}{\partial z}$$

in which

$\xi = X_0 - X$

$\eta = Y_0 - Y$

$\zeta = Z_0 - Z$

$\beta = \sqrt{M^2 - 1}$

$M$ = Mach number

and $-\ell_x, \ell_y, \ell_z$ are the direction cosines of the conormal to the influencing surface and $\ell_x$, $\ell_y$, and $\ell_z$ are the direction cosines of the inward drawn normal to the surface.

Writing the exponential term denoted by Eq. (3) in the product form, the potential gradient method of Refs. 7 and 8 can now be derived in terms of the pressure differential. Let

$$\exp[(ikM^2/\beta^2)X] = \exp(ikX)\exp[(ik/\beta^2)X]$$

and integrating by parts, Eq. (5) can be rewritten as

$$\phi(X_0) = E\iint\frac{\partial K}{\partial X}\frac{\partial P}{\partial n}\,\mathrm{d}\xi\,\mathrm{d}\eta \tag{6}$$

where

$$P = \exp(-ik\xi)\int_{\beta r}^{\xi}\exp(ik\xi'/\beta^2)\left(\frac{\cos k'R'}{R'}\right)\mathrm{d}\xi' \tag{7}$$

and

$$\frac{\partial K}{\partial X} = \frac{\partial\Delta\phi}{\partial x} + ik\Delta\phi, = -\Delta C_p \tag{8}$$

is the new variable in which $\Delta\phi = \phi_U - \phi_L$ is the circulation, and $\Delta C_p = C_{p_U} - C_{p_L}$ is the difference in the pressure between the upper and lower surfaces. Unlike in Refs. 7–10, there is no need to consider the influence of the wake, since $\Delta C_p$ is zero in the wake.

The closed-form evaluation of the integral in Eq. (6) is not possible for general planforms; hence, a numerical integration scheme using a discrete number of panels is employed with uniform distribution of $\Delta C_p$ over each panel. Then the velocity potential for a unit value of $\Delta C_p$ is given by

$$\phi = -E\int_{\xi_L}^{\xi_U}\int_{n_L}^{n_U}\frac{\partial P}{\partial n}\,\mathrm{d}\xi\,\mathrm{d}\eta \tag{9}$$

where $\xi_U,\xi_L$ and $\eta_U,\eta_L$ are the upper and lower limits of the panels in the $\xi$ and $\eta$ directions, respectively.

The normal-wash $w_{ij}$ at a control point $i$ due to a unit pressure at the $j$th element can be expressed as follows:

$$w_{ij} = -E\int_{\eta_L}^{\eta_U}\int_{\xi_L}^{\xi_U}\frac{\partial}{\partial n_0}\left(\frac{\partial P}{\partial n}\right)\mathrm{d}\xi\,\mathrm{d}\eta \tag{10}$$

where

$$\frac{\partial}{\partial n_0} = \ell_{x_0}\frac{\partial}{\partial x_0} + \ell_{y_0}\frac{\partial}{\partial y_0} + \ell_{z_0}\frac{\partial}{\partial z_0} \tag{11}$$

in which $\ell_{x_0}$, $\ell_{y_0}$, and $\ell_{z_0}$ are the direction cosines of the normal at the control panel. The relation between the pressure and the normal wash condition is written as

$$\{\Delta C_p\} = [A]\left\{\frac{\mathrm{D}\eta}{\mathrm{D}T}\right\} \tag{12}$$

where

$$A = [w_{ij}]^{-1} \tag{13}$$

is an aerodynamic influence coefficient (AIC) matrix and

$$\frac{\mathrm{D}\eta_n}{\mathrm{D}T} = \frac{\partial\eta_n}{\partial X} + ik\eta_n \tag{14}$$

is the kinematic nondimensional downwash due to the $n$th mode. Finally, the generalized aerodynamic work coefficient in the vibration mode $m$ due to the $n$th pressure mode, from the principle of virtual work, is given by

$$Q_{mn} = q\ell^3\iint_S \eta_m\Delta C_{p_n}\,\mathrm{d}\xi\,\mathrm{d}\eta \tag{15}$$

where $q = \frac{1}{2}\rho V^2$ is the dynamic pressure and $S$ the total area of the lifting surfaces.

## Evaluation of the Velocity Influence Coefficients

In the following analysis, the lifting surfaces will be assumed to lie in the stream direction (i.e., $\ell_x = 0$). Then the differential operator of Eq. (10) can be written as

$$\frac{\partial^2 P}{\partial n_0\partial n} = C_1\frac{1}{r}\frac{\partial P}{\partial r} + C_2\frac{1}{r_c}\frac{\partial}{\partial r_c}\left(\frac{1}{r}\frac{\partial P}{\partial r}\right) \tag{16}$$

where

$$C_1 = (\ell_z\ell_{z_0} + \ell_y\ell_{y_0}) \tag{17}$$

$$C_2 = [\zeta^2\ell_z\ell_{z_0} + \eta^2\ell_y\ell_{y_0} + \eta\zeta(\ell_z\ell_{y_0} + \ell_y\ell_{z_0})] \tag{18}$$

and $r_c = \sqrt{\eta_c^2 + \zeta_c^2}$ is the cross-flow distance between the center of the influencing element and the control point.

Differentiating $P$ with respect to $r$ and integrating by parts with respect to $\xi$ gives

$$\frac{1}{r}\frac{\partial P}{\partial r} = H_0 \tag{19}$$

where $H_0$ is given by

$$H_0 = \exp(-ik\xi)\left[\frac{\xi}{r^2R}\exp(-ik\xi/\beta^2)\cos k'R + i\frac{kr}{2r^2}\int_{(\xi-MR)/\beta^2 r}^{(\xi+MR)/\beta^2 r}\frac{T}{\sqrt{T^2+1}}\exp(-ikrT)\,\mathrm{d}T\right] \tag{20}$$

where

$$T = \frac{\xi \pm MR}{\beta^2 r} \tag{21}$$

For $\zeta = 0$, $H_0$ reduces to the planar kernel function derived by Watkins and Berman[17] using the acceleration potential method.

The integration of the second term in Eq. (20) can be performed using an approximation similar to the one used in the doublet-lattice method,[1] i.e.,

$$\frac{T}{\sqrt{T^2+1}} \doteq \left[1 - \sum_{m=1}^{N} a_m\exp(-2^m bT\delta)\right]\delta \tag{22}$$

where $\delta = \mathrm{sgn}(\xi - MR)1$.

The constants of the series from Ref. 18 for $N = 8$ are given as follows:

$$b = 0.0350039075,\ a_1 = 0.00432952,\ a_2 = 0.00160137$$

$$a_3 = 0.033195,\ a_4 = 0.0986923,\ a_5 = 0.37673986$$

$$a_6 = 0.822464,\ a_7 = -0.3802627,\ a_8 = 0.04340039$$

Substituting Eq. (22) into Eq. (20) and integrating, one obtains for the $H_0$ function,

$$\begin{aligned} H_0 = {} & \exp(-ik\xi)\left(\frac{\xi}{r^2R}\exp[-i(k/\beta^2)\xi]\cos k'R\right. \\ & + \frac{1}{2r^2}\{\delta\exp[-i(k/\beta^2)(\xi - MR)\} - \exp[-i(k/\beta^2)(\xi + MR)]\Big) \\ & + \frac{ikr}{2r^2}\exp(-ik\xi)\sum_{m=1}^{m=N} a_m\Big(\{\exp[-2^m b(\xi + MR)/\beta^2 r] \\ & \times \exp[-i(k/\beta^2)(\xi + MR)] - \delta\}/D_1 \\ & + \{\delta - \exp[(-2^m b|\xi - MR|)/\beta^2 r] \\ & \times \exp[-i(k/\beta^2)(\xi - MR)]\}/D_2\Big) \end{aligned} \tag{23}$$

where

$$D_1 = 2^m b + ikr \quad \text{and} \quad D_2 = \delta 2^m b + ikr$$

The kernel $H_0$ contains two types of singularities, namely: one of the hyperbolic nature along the forward Mach cone as $R$ approaches zero, and the other a dipole singularity as $r$ approaches zero, which is common to both subsonic and supersonic flow. The hyperbolic singularity is eliminated in the present approach by performing the first integration in the streamwise direction, by which the resulting function is rendered analytic on the Mach boundary. A similar integration scheme was employed in Refs. 7 and 8 to obtain the closed-form solutions for the downwash terms.

The dipole singularity can be treated by the application of the principal value theorem, as discussed in the next section. The derivation of the normal velocity component is given as follows.

Substituting the expression of Eq. (16) into Eq. (10), the normal-wash can be written as

$$w_{ij} = E\left[C_1 w_1 + C_2\frac{1}{r_c}\frac{\partial w_1}{\partial r_c}\right] \tag{24}$$

where

$$w_1 = \int_{\eta_L}^{\eta_U}\int_{\xi_L}^{\xi_U} H_0\,\mathrm{d}\xi\,\mathrm{d}\eta \tag{25}$$

Integrating Eq. (25) with respect to $\xi$, the normal-wash component $w_1$ is then given by

$$w_1 = \int_{\eta_L}^{\eta_U}\frac{F(\eta)}{r^2}\,\mathrm{d}\eta \tag{26}$$

where

$$F(\eta) = \left[\frac{\exp(-ik'M\xi)\,\sin k'R}{k'}\right]_{\xi_L}^{\xi_U} + iM\int_{\xi_L}^{\xi_U}\exp(-ik'M\xi)\,\sin k'R\,d\xi + \int_{\xi_L}^{\xi_U}\tfrac{1}{2}\exp(-ik\xi)\Big(\delta\{\exp[-i(k/\beta^2)(\xi - MR)] - 1\} + \{1 - \exp[-i(k/\beta^2)(\xi + MR)]\} + ikr\sum_{m=1}^{m=N} a_m \times \{\exp[-2^m b(\xi + MR)/\beta^2 r] \times \exp[-i(k/\beta^2)(\xi + MR)] - 1\}/D_1 + \delta\{1 - \exp[-2^m b|\xi - MR|/\beta^2 r] \times \exp[-i(k/\beta^2)(\xi - MR)]\}/D_2\Big)\,d\xi \quad (27)$$

The function $F(\eta)$ is now rendered nonsingular, unlike the kernel functions employed in other methods (e.g., Refs. 11–15). Since the second and third terms are nonsingular, numerical integrations using Gaussian quadrature can be performed.

The spanwise integration of Eq. (26) contains a dipole singularity. Since the numerator is analytic, this term can be expressed as a polynomial and integrated in a closed form using the principal value theorem. The second term in Eq. (24) needs to be evaluated for out-of-plane interfering elements. Since $w_1$ can be evaluated at any control point and it is continuous, the contribution from the second term can be determined by evaluating $w_1$ at two points normal to the panel containing the control point, and taking the finite difference of $w_1$ at the control point.

A similar finite-difference scheme was used in Ref. 15 to determine the normal velocity with good correlation with other methods. The evaluation of the functions can be performed on any triangular or quadrilateral panels. For the sake of computational convenience, the side edges are considered to be parallel to the streamlines.

## Discussion of Results

To verify the accuracy and reliability of the constant pressure method (CPM), a few examples are chosen to evaluate the pressure distributions and the generalized aerodynamic force coefficients.

The first set of examples compares the predicted pressure distributions resulting from high-frequency oscillations in heave and pitch modes. The computed data are compared with the two-dimensional solutions reported in Ref. 19. A rectangular wing with an aspect ratio of 4.0 was used with 20 chordwise and 10 spanwise elements. At Mach number $M = 1.25$, the Mach wave emanating from the side edge intersects the trailing edge at 33% span. Hence, the pressure distribution within the inboard 30% of the span behaves like the two-dimensional flow, which can be compared with exact two-dimensional solutions.

Figures 1 and 2 show the in-phase and out-of-phase chordwise pressure distributions for the heave motion. The solid

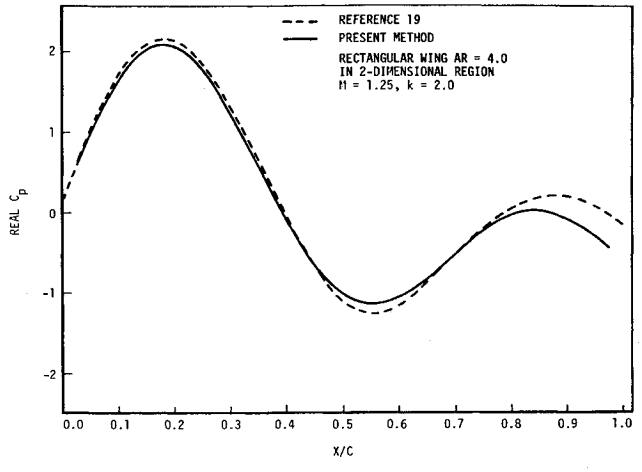


Fig. 1 Correlation of the in-phase pressure in heave.

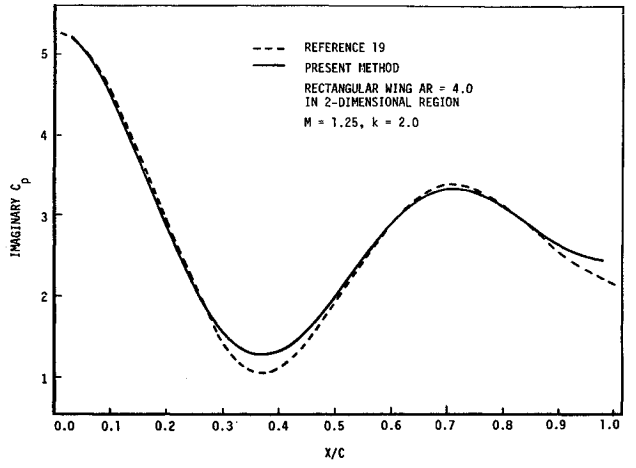


Fig. 2 Correlation of the out-of-phase pressure in heave.

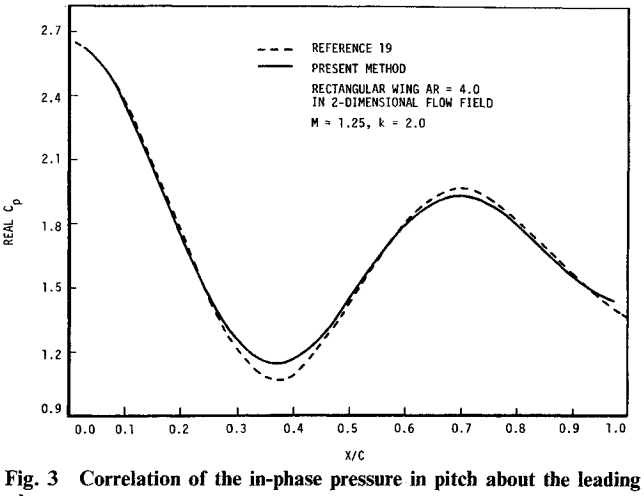


Fig. 3 Correlation of the in-phase pressure in pitch about the leading edge.

Table 1 Convergence study of the generalized forces on AGARD swept wing configuration at $M = 1.04$, $k = 1.0$; (mode $Z_1$ = heave, $Z_2$ = pitch about midchord)

| Generalized coefficients | Ref. 20 30 × 18 | Ref. 3 30 × 10 | Present 10 × 5 | Present 10 × 10 | Present 20 × 10 |
|---|---|---|---|---|---|
| | | | In phase | | |
| $Q_{11}$ | −0.5030 | −0.6100 | −0.5012 | −0.56710 | −0.5674 |
| $Q_{21}$ | −0.8330 | −0.8604 | −0.7694 | −0.8491 | −0.8491 |
| $Q_{12}$ | 4.935 | 4.6815 | 4.6780 | 4.752 | 4.7680 |
| $Q_{22}$ | 1.0360 | 0.9645 | 0.9873 | 0.9625 | 0.9672 |
| | | | Out of phase | | |
| $Q_{11}$ | 4.1300 | 3.9124 | 3.9340 | 4.010 | 4.0060 |
| $Q_{12}$ | 0.674 | 0.6180 | 0.7079 | 0.6485 | 0.6392 |
| $Q_{12}$ | 2.0510 | 2.0873 | 2.2240 | 2.1380 | 2.1410 |
| $Q_{22}$ | 2.1020 | 2.0629 | 2.0180 | 2.084 | 2.1010 |

**Table 2 Correlation of generalized aerodynamic coefficients for AGARD wing-tail configuration ($M = 1.414$, $k = 1.5$, $Q = Q' + ikQ''$, $Z = 0.0$)**

| | | Wing | | | | Tail | | | | |
|---|---|---|---|---|---|---|---|---|---|---|
| | | 1 | | 2 | | 3 | | 4 | | |
| | Mode | $Q'$ | $Q''$ | $Q'$ | $Q''$ | $Q'$ | $Q''$ | $Q'$ | $Q''$ | References |
| Wing | 1 | −0.2491 | 0.2894 | −0.3812 | 1.3818 | 0.0009 | 0.0 | 0.0013 | −0.0014 | Ref. 2 |
| | | −0.2770 | 0.2972 | −0.4360 | 1.4327 | 0.0054 | 0.0013 | 0.0073 | −0.0042 | Present |
| | 2 | −0.9613 | 1.0195 | −1.4526 | 5.1506 | 0.0035 | 0.0 | 0.0049 | −0.0055 | Ref. 2 |
| | | −1.0770 | 1.0307 | −1.9660 | 5.2750 | 0.0205 | 0.0029 | 0.0276 | −0.0164 | Present |
| Tail | 3 | −0.2117 | −0.1028 | −1.0347 | −0.2791 | −0.0120 | 0.2146 | 0.3421 | 0.3715 | Ref. 2 |
| | | 0.2149 | −0.0076 | −1.0460 | −0.2822 | −0.0176 | 0.2231 | 0.3366 | 0.3973 | Present |
| | 4 | −0.3196 | −0.1163 | −1.4934 | −0.2505 | −0.0296 | 0.3253 | 0.5248 | 0.6204 | Ref. 2 |
| | | −0.3234 | −0.1244 | −1.5140 | −0.2603 | −0.0390 | 0.3366 | 0.5093 | 0.6576 | Present |

Note: For mode 1: wing $Y^2$, tail 0.0; for mode 2: wing $XY$, tail 0.0; for mode 3: wing 0.0, tail $Y^2$; for mode 4: wing 0.0, tail $Y(X - 2.7)$. All antisymmetric.

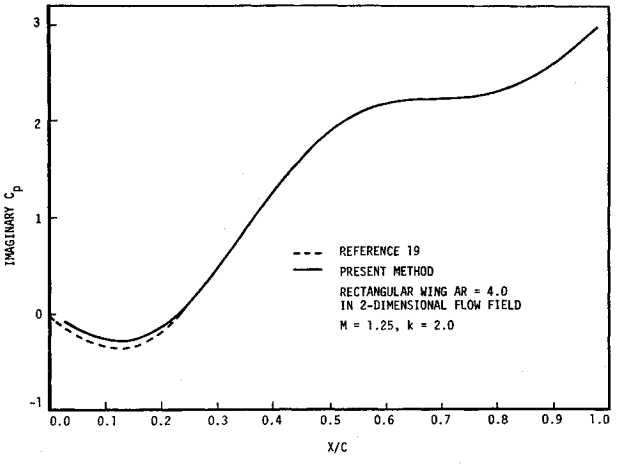


**Fig. 4 Correlation of the out-of-phase component of the pressure in pitch about the leading edge.**

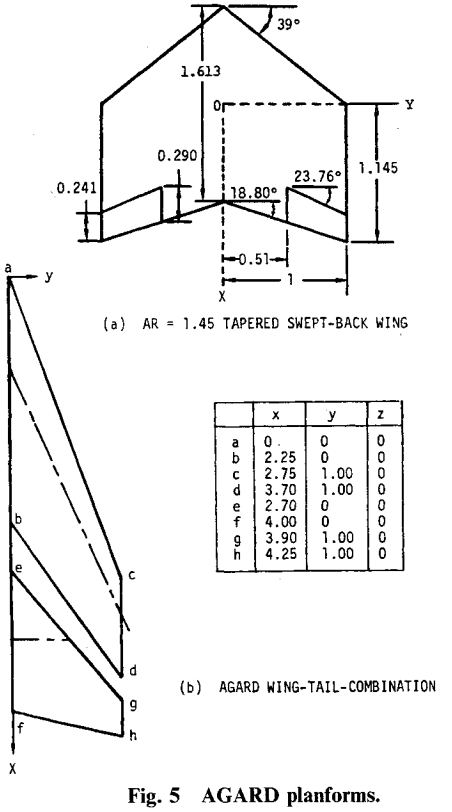


| | x | y | z |
|---|---|---|---|
| a | 0 | 0 | 0 |
| b | 2.25 | 0 | 0 |
| c | 2.75 | 1.00 | 0 |
| d | 3.70 | 1.00 | 0 |
| e | 2.70 | 0 | 0 |
| f | 4.00 | 0 | 0 |
| g | 3.90 | 1.00 | 0 |
| h | 4.25 | 1.00 | 0 |

**Fig. 5 AGARD planforms.**

lines represent the data computed from the CPM code, while the dotted lines indicate the corresponding data taken from Ref. 19. The agreement is seen to be very good except for some deviation at the trailing edge, which may be due to the finiteness of the model used in the present analysis. Since panels are not aligned in the Mach line directions, some panels lie partially in the two- and three-dimensional regions.

The in-phase and out-of-phase pressure distributions computed for the pitching motion about the leading edge are shown in Figs. 3 and 4, respectively. Once again, the agreement is seen to be very good.

The next set of data, shown in Table 1, demonstrates the rate of convergence of the generalized aerodynamic coefficients on the AGARD swept wing planform (Fig. 5a) in heave and pitching motion at a reduced frequency of $k = 1.0$ at $M = 1.04$. The generalized force coefficients were computed using $10 \times 5$, $10 \times 10$, and $20 \times 10$ chordwise and spanwise panel arrangements. A minimum of 10 panels in the chordwise direction was required to represent properly the chordwise variation of the pressure at $k = 1.0$. The in-phase and out-of-phase components of the generalized coefficients are compared with the results of Refs. 3 and 20. The convergence is very rapid. The data obtained from the $10 \times 5$ panel arrangement are also in good agreement with the reference data.

Figure 6 shows the variation of the in-phase and the quadrature components of the lift and moment coefficients on a rectangular wing as a function of the reduced frequency. The wing was modeled with 15 panels in the stream direction and 10 elements in the spanwise directions. The computations were performed for pitching motion about the midchord at $M = 1.05$ for $k = 0.0$–$2.0$. The solid and chain lines denote the results of Ref. 21, while the solid dots represent the data from the present method. The agreement is seen to be very good.

To verify the interference effects, computations were performed on AGARD wing-tail configurations shown in Fig. 5b, using uncoupled modes for wing and tail components. Table 2 shows the correlation of the generalized forces for the coplanar configuration in which the streamwise separation at the centerline ($X_{TLE} - X_{WTE}$) was 0.25. The deformation modes used in this analysis represent wing bending, wing twisting, tail bending, and tail twisting in antisymmetric oscillation. The computations were performed using $10 \times 10$ panels on the wing and $10 \times 10$ panels on the tail at $M = 1.414$ and $k = 1.5$. The results of Ref. 2, which employed the Mach box method using subdivided panel arrangements and a smoothing technique, are shown in the first row of each mode. The generalized coefficients obtained from the present method agree well with those of Ref. 2, except for the tail interference on the wing. The magnitudes of these terms are very small compared to the coefficients on the wing due to wing modes or on the tail due to tail modes. The discrepancy might arise either due to modeling

**Table 3 Correlation of generalized aerodynamic coefficients for AGARD wing-tail configuration ($M = 1.2$, $k = 1.5$, $Q = Q' + ikQ''$, $Z = 0.6$)**

| | | Wing | | | | Tail | | | | |
|---|---|---|---|---|---|---|---|---|---|---|
| | | 1 | | 2 | | 3 | | 4 | | |
| | Mode | $Q'$ | $Q''$ | $Q'$ | $Q''$ | $Q'$ | $Q''$ | $Q'$ | $Q''$ | References |
| Wing | 1 | −0.3458 | 0.2870 | 0.4123 | 0.4569 | — | — | — | — | Ref. 22 |
| | | −0.3548 | 0.3064 | 0.4051 | 0.4833 | — | — | — | — | Present |
| | 2 | −0.1722 | −0.0151 | −0.1245 | 0.2847 | — | — | — | — | Ref. 22 |
| | | −0.2003 | −0.0151 | −0.1565 | 0.2873 | — | — | — | — | Present |
| Tail | 3 | −0.0168 | 0.0038 | −0.0195 | 0.0160 | −0.1093 | 0.4945 | 1.0194 | 0.5892 | Ref. 22 |
| | | 0.0177 | −0.0076 | 0.0186 | −0.0287 | −0.0999 | 0.5019 | 1.0150 | 0.5956 | Present |
| | 4 | 0.0269 | 0.0243 | 0.0585 | −0.0133 | −0.1663 | 0.2955 | 0.4834 | 0.6518 | Ref. 22 |
| | | 0.0352 | 0.0222 | 0.0621 | −0.0131 | −0.1628 | 0.3050 | 0.4878 | 0.6649 | Present |

Note: For mode 1: wing $Y^2$, tail 0.0; for mode 2: wing $Y(X - 2.25/y/ - 0.85)$, tail 0.0; for mode 3: wing 0.0, tail $Y$; for mode 4: wing 0.0, tail $X - 3.35$. All antisymmetric.

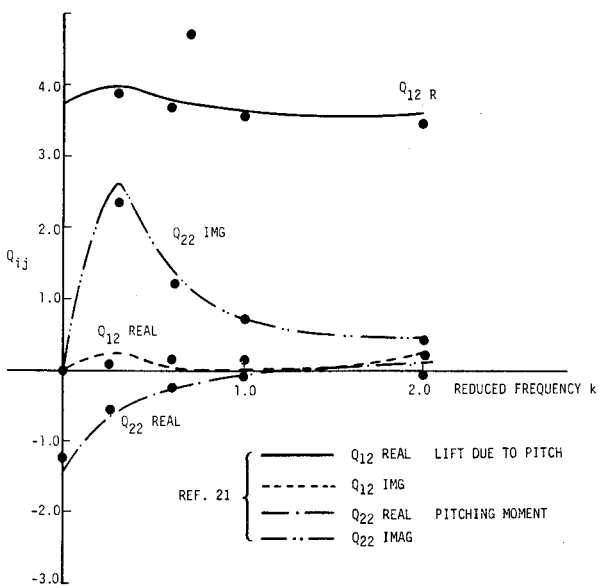


**Fig. 6 Variation of the computed generalized forces on a rectangular wing of aspect ratio 4.0 with the reduced frequency $k$, at $M = 1.04$.**

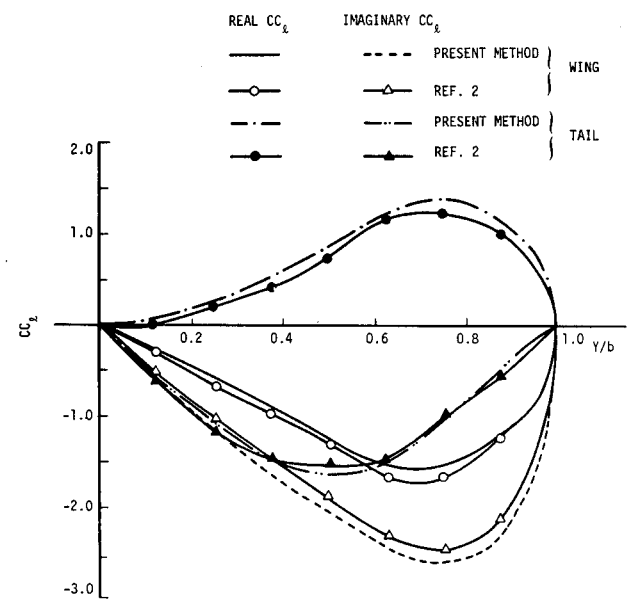


**Fig. 7 Correlation of the spanwise lift distribution due to antisymmetric wing twist (coplanar case); $M = 1.2$, $k = 1.5$.**

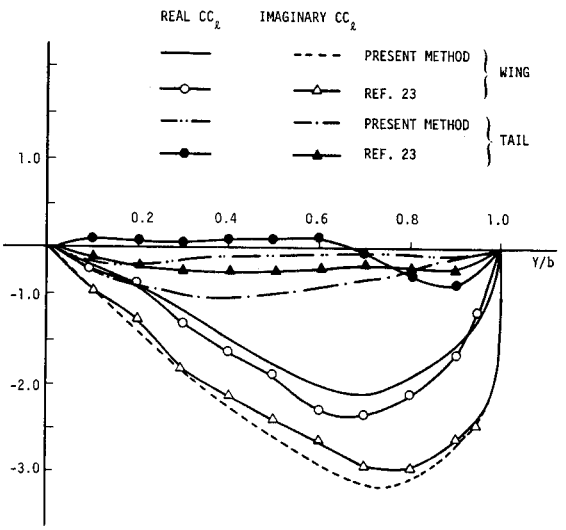


**Fig. 8 Correlation of spanwise lift distribution due to antisymmetric wing twist with tail dihedral = 30 deg and $(Z_{tail} - Z_{wing}) = 0.0$; $M = 1.2$, $k = 1.5$.**

differences or the computational inaccuracy in the Mach box method, which employs the computation over the diaphragm regions.

The results of nonplanar configurations with streamwise separation of $X_{TLE} - X_{WTE} = 0.65$ and vertical separation of $Z_{tail} - Z_{wing} = 0.6$ are given in Table 3. Antisymmetric vibration modes such as wing bending, wing twisting, tail rolling, and tail pitching were used. At $M = 1.2$, the wing was unaffected by the tail motion. The results of the present method compare very well with those reported in Ref. 22, except for some variation in the $Q''_{31}$ and $Q'_{41}$ components.

The next two examples compare the spanwise lift distributions ($CC_\ell$) on the coplanar and noncoplanar configurations, due to antisymmetric wing twisting. Figure 7 shows the correlation of the in-phase and quadrature components of the $CC_\ell$ distribution on the wing and tail components. The results of the present method are denoted by solid, dotted, and chain lines; whereas the data of Ref. 2 are given by the open and solid symbols. The lift distributions on the wing and tail components are in good agreement with the referenced data.

The noncoplanar configuration with the tail dihedral angle of 30 deg and $(Z_{tail} - Z_{wing}) = 0$ at $y = 0$ was employed to compute the lift distributions shown in Fig. 8. The lift distribution on the wing agrees reasonably well with the results of Ref. 18. However, the quadrature component of lift distribution on the tail is higher than that from Ref. 18, while the in-phase component has an opposite sign. In the absence of a third data source,

it is difficult to judge which data are good. In earlier examples in Tables 2 and 3, the generalized coefficients on tail components due to wing motion are seen to be very good. It is, therefore, possible that the modeling of the diaphragm elements in the dihedral configuration might have caused some computational inaccuracies in the results of Ref. 2.

## Conclusion

The constant pressure method presents a direct approach for the computation of the unsteady aerodynamic loads on wing-tail configurations of arbitrary configurations, without the need for the consideration of wake or the diaphragm regions. The results presented in this paper demonstrate the accuracy and computational efficiency of the present method for arbitrary planforms. Since the constant pressure method is similar to the doublet-lattice (DLM) code employed in subsonic analysis, the constant pressure method (CPM) subroutine, which computes the influence coefficients, can be directly integrated into the DLM code, such that there is no change in the input or output formats. Thus, a unified code would then be available for subsonic and supersonic analyses.

## References

[1]Rodden, W. P., Giesing, J. P., and Kalman, T. P., "New Developments and Applications of the Subsonic Doublet-Lattice Method for Nonplanar Configurations," AGARD Symposium on Unsteady Aerodynamics for Aeroelastic Analysis of Interfering Surfaces, AGARD CP-80-71, Nov. 1970.

[2]Ii, J. M., Borland, C. J., and Hogley, J. R., "Prediction of Unsteady Aerodynamic Loadings of Nonplanar Wings and Wing-Tail Configurations in Supersonic Flow; Part 1, Theoretical Development, Program Usage and Application," AFFDL-TR-71-108, Pt. I, March 1972.

[3]Stark, V. J. E., "Calculation of Aerodynamic Forces on Two Oscillatory Finite Wings at Low Supersonic Mach Numbers," SAAB TN 53, 1964.

[4]Appa, K., "Kinematically Consistent Unsteady Aerodynamic Coefficients in Supersonic Flow," *International Journal for Numerical Methods in Engineering*, Vol. 2, 1970, pp. 495–507.

[5]Woodcock, D. L. and York, E. J., "A Supersonic Box Collocation Method for the Calculation of Unsteady Airforces of Tandem Surfaces," AGARD-CP-80-71, Pt. I, 1971.

[6]Giesing, J. P. and Kalman, T. P., "Oscillatory Supersonic Lifting Surface Theory Using a Finite Element Doublet Representation," AIAA Paper 75-761, May 1975.

[7]Jones, W. P. and Appa, K., "Unsteady Supersonic Aerodynamic Theory for Interfering Surfaces by the Method of Potential Gradient," *AIAA Journal*, Vol. 15, Jan. 1977, pp. 59–65 (also NASA CR-2898, Oct. 1977).

[8]Appa, K. and Jones, W. P., "Three-Dimensional Unsteady Aerodynamic Analysis of Cascade Blades," Pratt and Whitney Group, PWA MR-11868, March 1980.

[9]Hounjet, M. H. L., "Improved Potential Gradient Method to Calculate Airloads on Oscillating Supersonic Interfering Surfaces," *Journal of Aircraft*, Vol. 19, May 1982, pp. 390–399.

[10]Chen, P. C. and Liu, D. D., "A Harmonic Gradient Method for Unsteady Supersonic Flow Calculations," *Journal of Aircraft*, Vol. 22, May 1985, pp. 371–379.

[11]Harder, R. L. and Rodden, W. P., "Kernel Function for Nonplanar Oscillating Surfaces in Supesonic Flow," *Journal of Aircraft*, Vol. 8, Aug. 1971.

[12]Cunningham, A.M., "Oscillatory Supersonic Kernel Function Method for Interfering Surfaces," *Journal of Aircraft*, Vol. 11, Nov. 1974, pp. 664–670.

[13]Brock, B. J. and Griffin, J. A. Jr., "The Supersonic Doublet-Lattice Method—A Comparison of Two Approaches," AIAA Paper 75–760, May 1975.

[14]Ueda, T. and Dowell, E. H., "Doublet-Point Method for Supersonic Unsteady Lifting Surfaces," *AIAA Journal*, Vol. 22, Feb. 1984.

[15]Lottati, I. and Nissim, E., "Nonplanar Supersonic Three-Dimensional Oscillatory Piecewise Continuous-Kernel Function Method," *Journal of Aircraft*, Vol. 24, Jan. 1987, pp. 45–54.

[16]Jones, W. P., "Supersonic Theory for Oscillating Wings of Any Planform," British ARC R & M 2655, June 1948.

[17]Watkins, C. E. and Berman, J. H., "On the Kernel Function of the Integral Equation Relating Lift and Downwash Distributions of Oscillatory Wings in Supersonic Flow," NACA Rept. 1257, 1956.

[18]Desmarais, R. N., "An Accurate and Efficient Method for Evaluating the Kernel of the Integral Equation Relating Pressure to Normalwash in Unsteady Potential Flow," *AIAA/ASME/ASCE/AHS 23rd Structures, Structural Dynamics and Materials Conference*, Pt. 2, May 1982.

[19]Jordan, P. F., "Aerodynamic Flutter Coefficients for Subsonic, Sonic and Supersonic Flow (Linear Two-Dimensional Theory)," ARC TR R & M 2932, 1957.

[20]Fenain, M. and Guiraud-Vallee, D., "Numerical Calculations of Wings in Steady or Unsteady Supersonic Flow, Part 1: Steady Flow, Part 2: Unsteady Flow," *Recherche Aerospatiale*, No. 115, 1966–1967.

[21]Woodcock, D. L., "Comparison of Methods Used in Lifting Surface Theory," AGARD Rept. 583, Jan. 1971.

[22]Rodden, W. P., "A Comparison of Methods Used in Interfering Lifting Surface Theory," AGARD Rept. 643, Feb. 1976.

[23]Pollock, S. S. and Huttsell, L. J., "Applications of Three Unsteady Aerodynamic Load Prediction Methods," AFFDL-TR-73-147, May 1974.